Non-Invasive Measurement of Central Aortic Pressure Through 4D Cardiac Ultrasound

Nidhi Srivaths[a], Kevin Xu[a], Jose Zarate[a]

[a]*Duke University, Dept. of Biomedical Engineering,*

Abstract

The measurement of central aortic pressure (CAP), i.e. the blood pressure at the aortic root, has recently been claimed to be a better indicator of hypertensive outcomes than traditional brachial cuff measurements. The standard for CAP measurement involves invasive arterial catheterization which impedes its widespread adoption particularly for non-urgent situations. This paper presents a method of non-invasively obtaining CAP by utilizing 4D cardiac ultrasound and image processing with MATLAB. Blood volume data in the left ventricle (LV) over the course of a heart cycle can be used to derive blood flow rate and flow acceleration into the aorta. Combined with the aortic cross sectional area (also obtained using cardiac ultrasound) and blood density, these measurements can be used to derive CAP. This approach yielded sensible CAP curves shape-wise during systole, making it a viable candidate for further testing and validation. Scaling was needed to match expected values from literature, likely due to unaccounted for factors including but not limited to blood viscosity, turbulent flow, and friction.

1. Introduction

1.1. Clinical Significance

The present standard of blood pressure (BP) measurement is the non-invasive measurement of brachial BP through cuff sphygmomanometry. Despite its popularity due to its legacy, ease of use, and the extensive nature of its diagnostic links, it is not fully representative of the body's true systemic pressure. A brachial blood pressure measurement is affected not only by the true aortic pressure, but also the stiffness of the arterial network leading into the arm.

The pressure at the aortic root connected to the left ventricle (LV), referred to as central aortic pressure (CAP), is the impedance the ventricle must overcome to pump blood, and is thus the pressure seen by target organs of systemic circulation. CAP is thus considered a better informer of medical inquiries such as response to beta blockers, diagnosis of hypertension and prediction of cardiovascular events. [4]

A significant barrier to the widespread use of CAP is the invasiveness of its current mode of measurement - arterial catheterization. This makes it impractical to use in large-scale clinical studies, limiting possible empirical validation of its use. In light of CAP's suggested superior diagnostic power, this paper presents an ultrasound based, non-invasive alternative to obtaining this measurement.

1.2. Present Work

Most non-invasive techniques for CAP measurement use an algorithm based approach, where the pressure of an accessible major artery like the carotid is obtained through tonometry [1], and the CAP is estimated from it. However, these approaches are highly susceptible to common pitfalls of machine learning such as over-reliance on historic data, lack of training set diversity and the "black box" nature of the algorithm's "learning".

The presented method tries to mitigate these drawbacks by performing direct calculations. Limited work has been done to utilize imaging modalities to such as MR to relate physical movement of the heart to CAP readings [3], but this paper aims to utilize ultrasound, which is a more accessible modality.

2. Overview

2.1. Aortic Area:

This measurement is crucial as it represents the area where the blood pumped by the LV exerts its pressure. ΔV from the previous calculation is now considered the volume of blood that creates the aortic pressure. The cross sectional area of the aortic root is assumed to be

Submitted for the purposes of BME 543

constant through the cardiac cycle with no significant distension during systole. With the success of these steps and the knowledge of the frame rate of the scan being analyzed, pressure is measured as:

$$\begin{aligned}\Delta P(i) &= \frac{F}{A} = \frac{m \times a}{A} = \frac{\rho \Delta V \times a}{A} \\ &= \frac{\rho_b (V_3 - V_1)}{A} \times \frac{[(V_3 - V_2) - (V_2 - V_1)]}{A \times (\Delta t)^2} \\ &= \frac{\rho_b (V_3 - V_1) \times [(V_3 - V_2) - (V_2 - V_1)]}{A^2 \times (\Delta t)^2}\end{aligned}$$

where:

$$\begin{aligned}\rho_b &= \text{density of blood} = 1.04, \text{g/cm}^3, \\ V_i &= \text{volume extracted from frame } i, \\ A &= \text{area of the aortic root.}\end{aligned}$$

2.2. Reorientation of Data:

Our datasets, like true clinical datasets, were not aligned to the true long axis of the heart. Without proper orientation, any 2D slice extracted would be oblique to the long axis instead of parallel, and thus impair its diagnostic use.

2.3. Volume Extraction:

With the heart now rotated in the correct orientation, the next step is to extract the volume of the left ventricle from each available frame. The difference between volumes in consecutive frames is assumed to be the volume of blood ejected into the aorta.

3. Assumptions and Implications

This model relies on the following key assumptions about the patient's specific cardiac anatomy and function and the analysis of extracted data.

1. The region of the aorta under test is subject to plug flow, i.e., the velocity at any time is uniform across all points on the cross sectional area.
2. The cross sectional area of the region of the aorta under test does not change through the cardiac cycle
3. The model is only valid for ventricular systole, i.e., when the aortic valve is fully open and the LV is emptying into the aorta.
4. All blood exiting the LV goes into the aorta.
5. The pressure in the aorta is a function of only the blood volume through it.
6. The aortic pressure gradient is the only determinant of fluid flow.

4. Methods

The methods mentioned briefly in Section 2 are outlined in detail below.

4.1. Aortic Area

A function was written to extract the aortic area from the given dataset, which works as follows:

1. Height slices are iterated through until the user identifies the first clear appearance of the mitral valve, aorta, and apex.

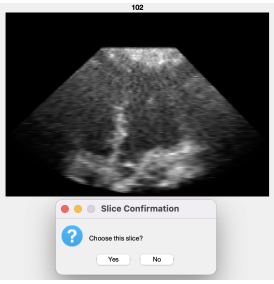

Figure 1 The current view shows slice 102 in the height dimension. The user is prompted to confirm whether the aorta is visible in this slice. If the aorta is not in view, the user can choose to navigate through the slices: advancing by either 1 or 10 frames in height, or moving back by 1 frame.

2. The user identifies the aorta, mitral valve, and apex. The three points are saved for processing.
3. The angle between the vectors formed by the selected points is calculated and the 3D data volume is rotated to align to the selected points.
4. The 3D dataset is rotated about the horizontal (width) axis in increments until the user indicates that the view of the aorta is head on, i.e. most circular shape.

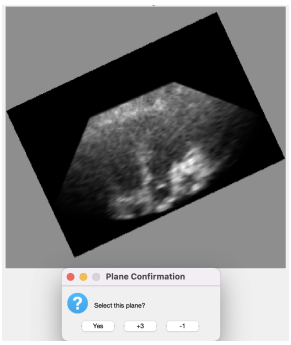

Figure 2 The current view shows a rotated slice with the aorta in view. The prompt asks the user if the aorta is fully circular. If it is, the user selects "Yes." If not, the user selects +3 or -1 to rotate the image 3° or 1° with the apex going into or out of the page, respectively.

5. Once satisfied by aorta viewing plane, the user now draws an aortic boundary, and the area within the boundary is reported in number of pixels. The is converted to physical dimensions by scaling by the known pixel to cm ratio of the dataset, which the function receives as input.

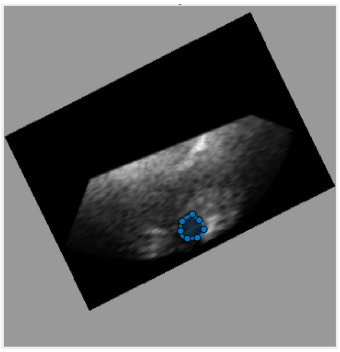

Figure 3 Using their cursor, the user drew an aortic boundary (shown in blue) and the program calculates the enclosed area.

4.2. Reorientation of Ventricle:

As the datasets were not necessarily oriented in the common diagnostic view, to ensure any clinical significance and consistency, a function was written and employed with the following key components:

1. The function initializes with the heart object and the cm/pixel information of the data as inputs. It extracts central slices of the heart volume along width, height, and depth dimensions for a given time frame.
2. These slices are displayed with different colored lines and borders for reference. The user is prompted to select a point at the mitral valve and another at the apex of the heart (i.e., the long axis of the heart).

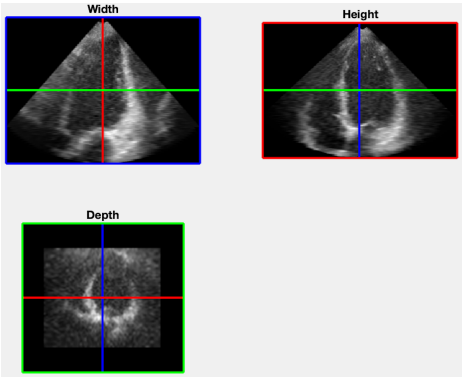

Figure 4

3. Based on user input, the function identifies which slice (width, height, or depth) the user interacted with. It calculates the midpoint and length of a line drawn by the user.

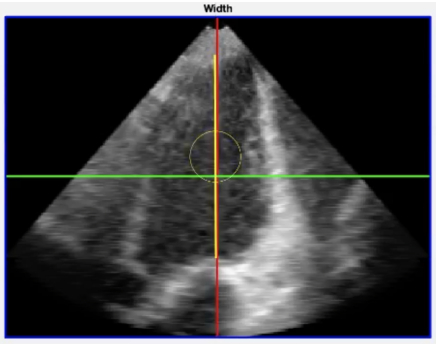

Figure 5

4. The function calculates translation distances and applies these to the original ventricular volume. This translation places the center of mass of the left ventricular volume (given by the drawn line's midpoint) with the center of the image.
5. The angle between the drawn line and the vertical axis is calculated, and the translated heart volume is rotated such that the line drawn becomes the new vertical axis.
6. The translated and rotated volume is cropped to match the original dimensions of the image.
7. The user provides additional input on two different depth slices of the reoriented volume. The function calculates a new rotation angle about the complementary axis to the first axis of rotation based on these input and applies it to the volume. The second rotation is done to further guarantee that the image is aligned vertically along the long axis.

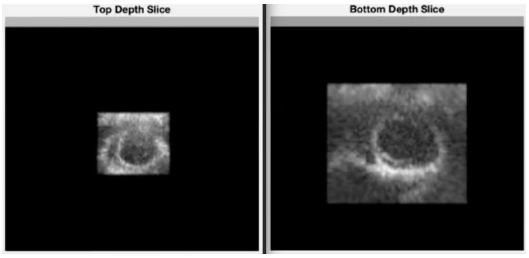

Figure 6 The user is instructed to select the centers of two distinct depth cross sections. The top slice is 20% into the depth dimension. The bottom slice is approximately 39% into the depth dimension. Selecting these two central points is intended to further align the ventricle.

8. The final output of the function is the translated, rotated and cropped (i.e., fully reoriented) LV volume (outputVolume) and the dimension selected by the user (selectedDimension).

Figure 7

4.3. Volume Extraction

1. 2D slices of the heart are extracted from the reoriented 3D dataset and each slice is displayed to the user. The user is prompted to draw a region enclosing the LV. The user also inputs points corresponding to the apex and mitral valve on the displayed slice.

Figure 8

2. Each slice is divided into different volume sectors and the function calculates the distance from the LV walls and the long axis in each sector. The left and right "radii" allow for the calculation of the volume of each sector, given the thickness between slices from the scan specifics.

3. The 3D volume is rotated 45° a total of four times and each time, the 2D slice is shown to the user to enclose the region. The volume for all sectors is calculated for each of these slices and summed into the final volume of the entire LV for any given time-point.

4.4. Pressure Calculation

$P(t)$ can be calculated by integrating dP/dt for the systolic period. dP/dt is a function of blood density, the aortic cross sectional areas, LV volumetric flow rate, and the LV volumetric flow acceleration.

4.4.1. Method 1

The discrete $V(t)$ obtained from data during systole was stored in an array. A modified volume array was created by prepending and appending the first and last volumes respectively three times each to the original volume array, and this modified volume array was used to create a 5th degree polynomial interpolation of $V(t)$. This modification was done so that the rate of change of the interpolant was flat at the start and end of systole, which corresponds with expected zero velocity blood outflow into the aorta. The volumetric flow rate and volumetric flow acceleration were obtained by differentiating the interpolant once and twice respectively.

4.4.2. Method 2

A discrete dV/dt was obtained by taking the difference between adjacent volumes during systole from the empirical data. A third degree polynomial fit was used to interpolate the discrete data. A third degree polynomial is less susceptible to Runge's phenomenon (wild oscillations of interpolants of higher order) which was more appropriate given the low amount of sample points and irregular, patternless behavior of discrete dV/dt that tend to occur. The volumetric flow acceleration was obtained by differentiating the interpolant.

4.4.3. Both Methods

The resulting dV/dt and d^2V/dt arrays obtained by interpolating using either method are technically still discrete data, but have many more data points than the number of frames in the original data set, which makes them behave like continuous data. Modifying the pressure equation, we get:

$$\begin{aligned}\Delta P(i) &= \rho\left(V(i+2) - V(i+1) + (V(i+1) - V(i))\right) \times V''(i) \\ &= \rho\left(\frac{V(i+2) - V(i+1)}{\Delta t} + \frac{V(i+1) - V(i)}{\Delta t}\right)\Delta t \times V''(i) \\ &= \rho\Delta t\left(V'(i+1) + V(i)\right)V''(i)\end{aligned}$$

Iterating through $V'(t)$ allows for the calculation of the P'(t) array.
Cumulative pressure is calculated by $P(t) = \int_0^t P'(t)\,dt$. This was done using trapezoidal summation. Conversion of $P(t)$, currently in deciPascals, was converted to

the clinically relevant scale of mmHg. Results were further scaled up to reflect expected data.

5. Results

The above methods were used on two of the provided datasets, **002A** and **021_1a**. These datasets were chosen as they represented "normal" patients, with no known pathologies introducing additional variables. Frame rate data was unknown for Patient 2, assumed to be 15 vps, and known to be 32 vps for Patient 21.

5.1. Method 1 on dataset 021_1a

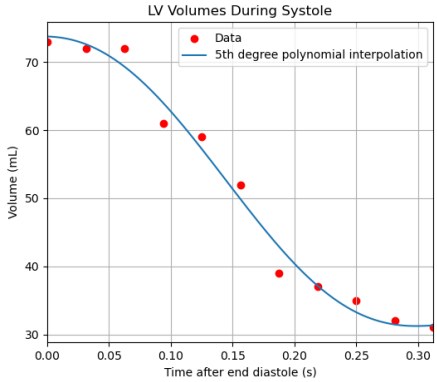

Figure 9

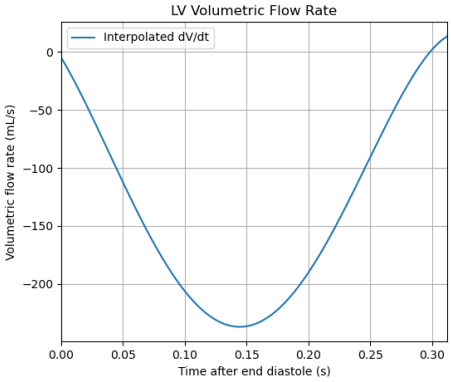

Figure 10

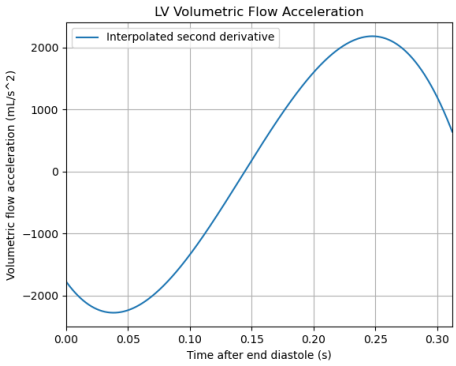

Figure 11

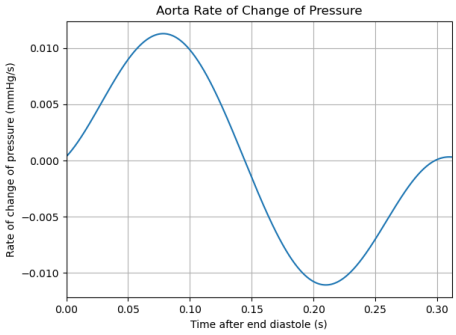

Figure 12

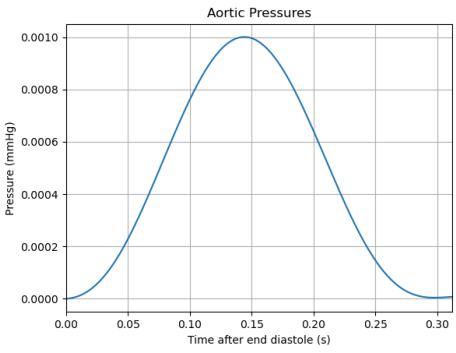

Figure 13

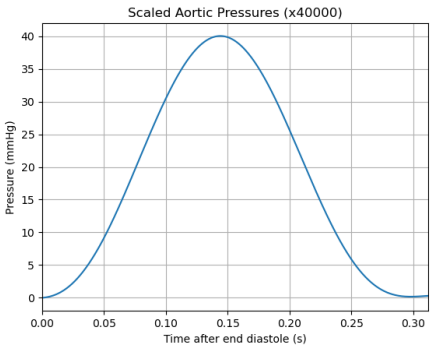

Figure 14

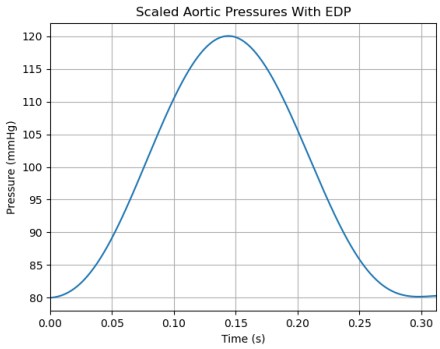

Figure 15

5.2. Method 2 on dataset 021_1a

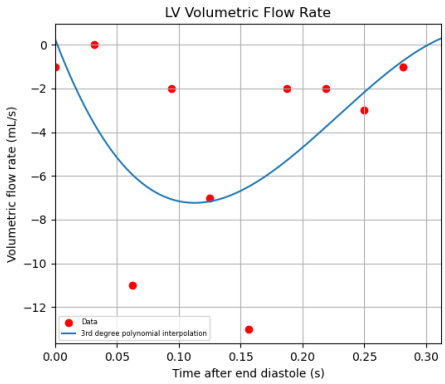

Figure 16

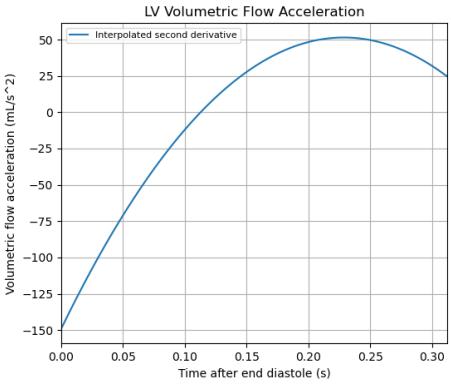

Figure 17

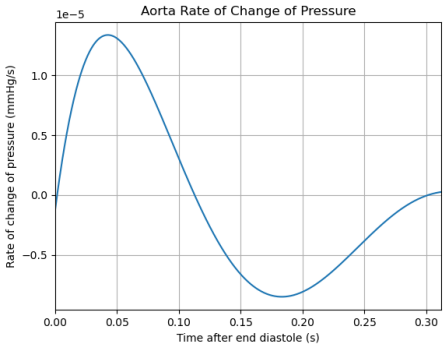

Figure 18

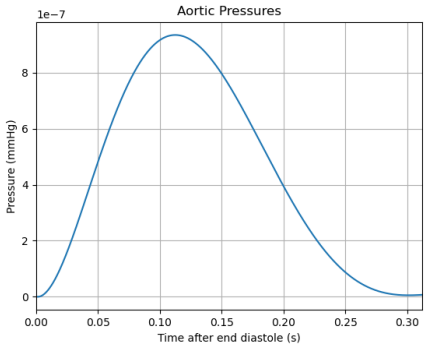

Figure 19

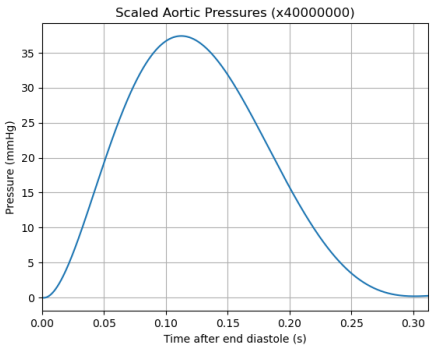

Figure 20

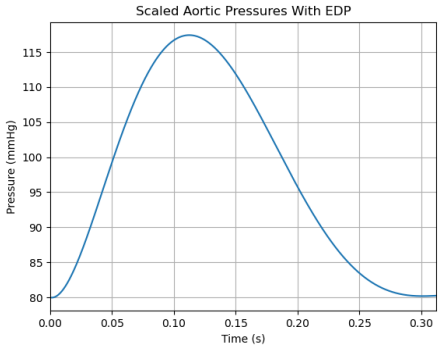

Figure 21

Note: Dataset 002A results are in **Appendix A** and the raw data for both datasets are in **Appendix B**.

6. Discussion

6.1. Limitations

The results above imply there are clear limitations of the model. An inherent limitation was the lack of correlative measurements in the dataset (like cuff pressure, patient history, etc.) for model calibration. and their implications on future work are discussed below:

1. The $P(t)$ graphs obtained using method 1 and method 2 had to be scaled up on the orders of tens of thousands and tens of millions respectively to get pressures comparable to reference sources. This differential can partly be explained by frictional forces between the blood and tissues, blood viscosity, and turbulent flow that may have opposed the pressure accelerating the blood. In short, the derived equation that measures the pressure is based on the acceleration of blood in an idealized environment without resistance, but in actuality there may have been significant resistances to blood flow that were not considered. However, the sheer order of magnitude of the scaling differential suggests that the model was missing some key component.

2. The biggest limitation of this approach lies in the fact a second derivative is needed, which magnifies any error in the initial volume measurements. Along with that error amplification, the model is also severely limited by the frame rate of the scan, which for one of the datasets is assumed to be around 15fps. This creates a wide interval between frames that are being analysed and especially at the beginning of systole, those missing frames create a clearly large discrepancy with the expected results.

3. Polynomial interpolation has an intrinsic disadvantage of exhibiting oscillating behavior at edge points known as Runge's phenomenon. Therefore, the true behavior of $V(t)$ in method 1 and dV/dt in method 2 may not be captured by the interpolant. These errors compound when calculating derivatives downstream until $V''(t)$. Since pressure is dependent on the second derivative of $V(t)$, any inaccurate reporting of V(t) or to a lesser degree $V'(t)$ will greatly affect $P(t)$ accuracy

6.2. Strengths

1. Pressure Trend: The shape of $P(t)$ matched reference aorta pressure during systole relatively well. Like reference curves, $P(t)$ was parabolic, maximized at or slightly after the mid-systole point, and reduced down to at or slightly above the EDP.

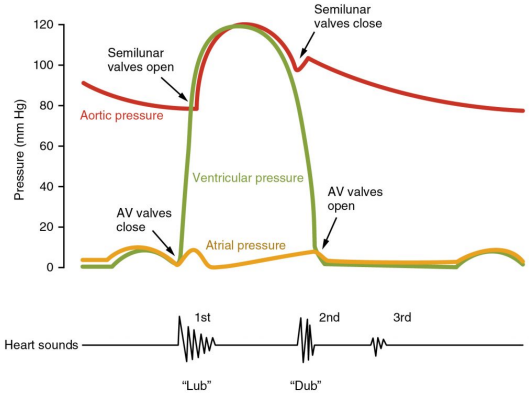

Figure 22 Wiggers diagram [2]

2. Proof of Concept: The derivation of $P(t)$ as a function of $V'(t)$, $V''(t)$, and constants blood density and aortic area is a baseline model which can be improved to derive $P(t)$. Future researchers can modify or add terms to account for phenomenon including mitral regurgitation, stenosis, turbulent flow, etc to obtain progressively better models that can more accurately report $P(t)$. Additionally, advances in ultrasound technology such as frame rate and resolution can be used to take advantage of more empirical data and rely less on interpolating functions.

Acknowledgements

The authors of this paper acknowledge the valuable contributions of BME 543 course instructors Dr. Olaf T. von Ramm and Dr. Joseph Kisslo for their expertise, Dr. Cooper Moore for his assistance, and Dr. Willard Applefeld for his advice.

References

1. C.-H. Chen et al., "Estimation of central aortic pressure waveform by mathematical transformation of radial tonometry pressure," Circulation, vol. 95, no. 7, pp. 1827–1836, 1997. doi:10.1161/01.cir.95.7.1827

2. J. G. Betts, Anatomy and Physiology — OpenStax," Apr. 25, 2013. https://openstax.org/books/anatomy-and-physiology/pages/1-introduction

3. L. Milne et al., "Central aortic blood pressure from ultrasound wall-tracking of the carotid artery in children," Hypertension, vol. 65, no. 5, pp. 1141–1146, 2015. doi:10.1161/hypertensionaha.115.05196

4. M. J. Roman et al., "Central pressure more strongly relates to vascular disease and outcome than does brachial pressure," Hypertension, vol. 50, no. 1, pp. 197–203, 2007. doi:10.1161/hypertensionaha.107.089078

Appendix A. Dataset 002A Results

Appendix A.1. Method 1 on dataset 002A

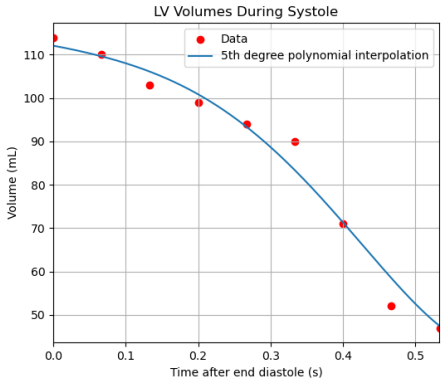

Figure A.23

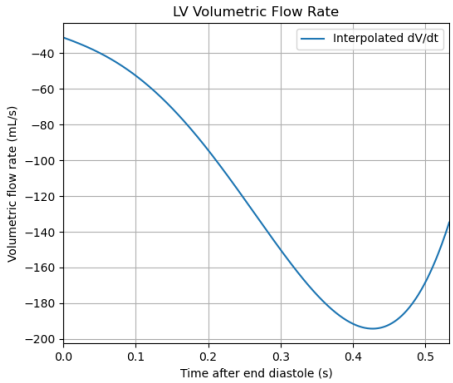

Figure A.24

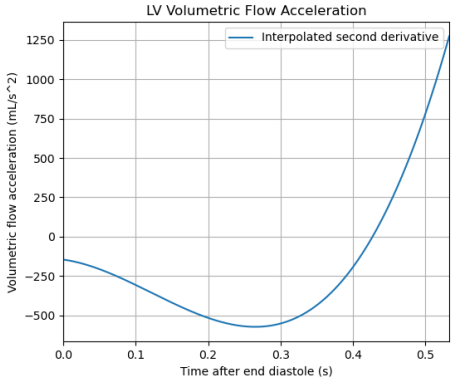

Figure A.25

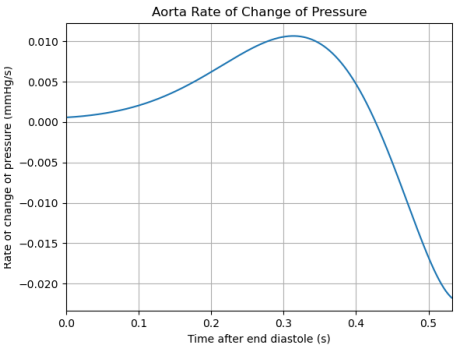

Figure A.26

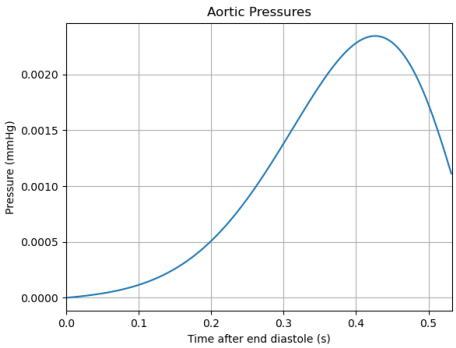

Figure A.27

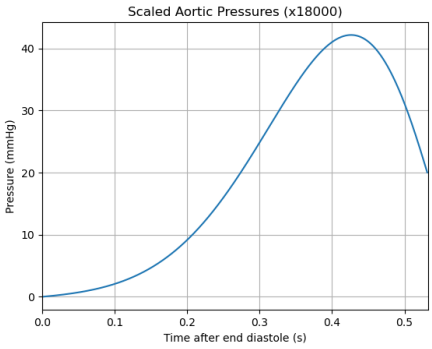

Figure A.28

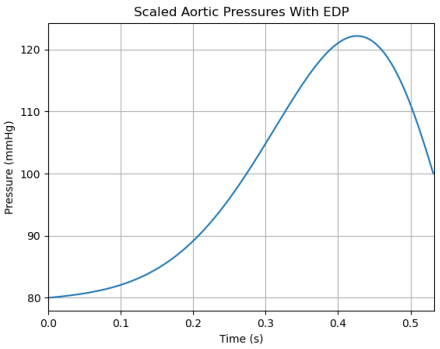

Figure A.29

Appendix A.2. Method 2 on dataset 002A

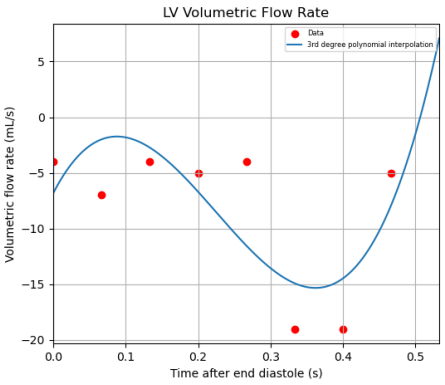

Figure A.30

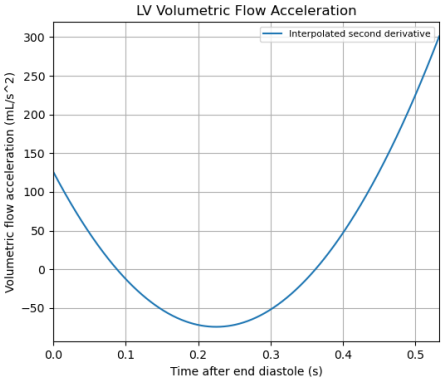

Figure A.31

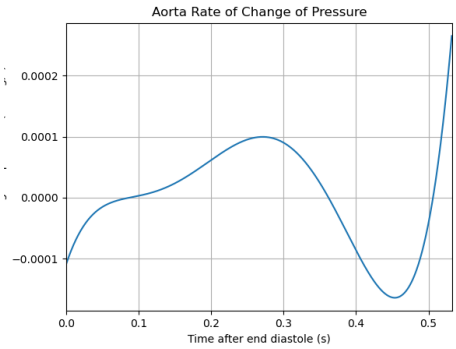

Figure A.32

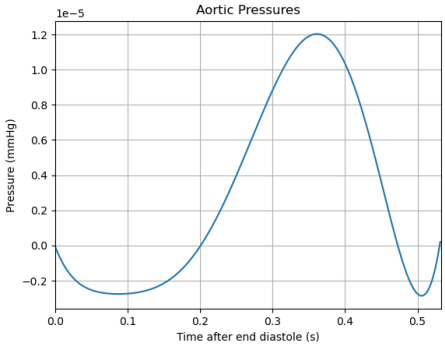

Figure A.33

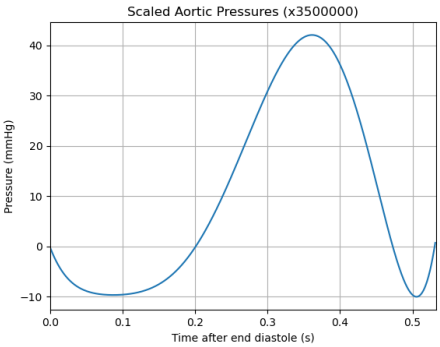

Figure A.34

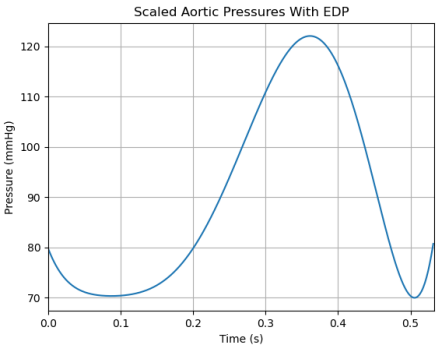

Figure A.35